Received: 22 June 2021 | Revised: 21 September 2021 | Accepted: 30 September 2021

DOI: 10.1002/mrm.29053

TECHNICAL NOTE

Magnetic Resonance in Medicine

Residual quadrupolar couplings observed in 7 Tesla deuterium MR spectra of skeletal muscle

Ayhan Gursan[1] | **Martijn Froeling**[1] | **Arjan D. Hendriks**[1] | **Dimitri Welting**[1] | **Arno P. M. Kentgens**[2] | **Dennis W. J. Klomp**[1] | **Jeanine J. Prompers**[1]

[1]Department of Radiology, University Medical Center Utrecht, Utrecht, The Netherlands

[2]Magnetic Resonance Research Center, Institute for Molecules and Materials, Radboud University, Nijmegen, The Netherlands

Correspondence
Jeanine J. Prompers, Department of Radiology, Division Imaging and Oncology, University Medical Center Utrecht, Heidelberglaan 100, 3584 CX, Utrecht, The Netherlands.
Email: J.J.Prompers@umcutrecht.nl

Funding information
This work was funded by a High Tech Systems and Materials (HTSM) grant from Dutch Research Council (NWO) - Toegepaste en Technische Wetenschappen (TTW) project number 17134; and by a Future and Emerging Technologies (FET) Innovation Launchpad grant from the EU, grant number 850488

Purpose: Deuterium metabolic imaging could potentially be used to investigate metabolism in skeletal muscle noninvasively. However, skeletal muscle is a tissue with a high degree of spatial organization. In this study, we investigated the effect of incomplete motional averaging on the naturally abundant deuterated water signal in 7 Tesla deuterium spectra of the lower leg muscles and the dependence on the angle between the muscle fibers and the main magnetic field B_0, as determined by DTI.

Methods: Natural abundance deuterium MRSI measurements of the right lower leg muscles were performed at 7 Tesla. Three subjects were scanned in a supine position, with the right leg parallel with the B_0 field. One subject was scanned twice; during the second scan, the subject was laying on his right side and the right knee was bent such that the angle between the right lower leg and B_0 was approximately 45°. DTI was performed in the same subjects in the same positions at 3 Tesla to determine muscle fiber angles.

Results: We observed splittings in the natural abundance deuterated water signal. The size of the splittings varied between different muscles in the lower leg but were mostly similar among subjects for each muscle. The splittings depended on the orientation of the muscle fibers with respect to the main magnetic field B_0.

Conclusion: Partial molecular alignment in skeletal muscle leads to residual deuteron quadrupolar couplings in deuterated water, the size of which depends on the angle between the muscle fibers and B_0.

KEYWORDS

deuterium MRS, deuterium metabolic imaging, muscle fiber angle, residual quadrupolar coupling, skeletal muscle

1 | INTRODUCTION

Deuterium metabolic imaging is a new technique to study tissue metabolism in vivo and has been applied in brain, liver, tumor, and brown adipose tissue.[1–7] Deuterium metabolic imaging is based on deuterium (^{2}H) MRSI (DMRSI) in combination with the administration of deuterated compounds such as deuterated glucose. This allows to spatially map the uptake of deuterated glucose in the tissue, as well as its conversion into metabolic products such as glutamate, glutamine, and lactate. In this way, rates of oxidative (mitochondrial) versus glycolytic metabolism can be estimated, the latter of which could potentially be used to assess tumor grade and response to therapy.[1,3]

In skeletal muscle, the assessment of mitochondrial metabolism has also been of interest for many years, especially in the context of insulin resistance and type 2 diabetes. In those studies, flux through the tricarboxylic acid cycle in the calf muscles has been determined using carbon-13 (^{13}C) MRS upon infusion of [2-^{13}C]acetate.[8–12] However, because of the low intrinsic sensitivity of ^{13}C MRS and the long T_1 relaxation times of ^{13}C nuclei, 3D mapping of ^{13}C-labeled metabolites using MRSI is not feasible, and the signal is usually acquired from a single large volume using unlocalized or slice-selected MRS.

Deuterium metabolic imaging in combination with administration of deuterated acetate could potentially be a more sensitive (and lower-cost) alternative to ^{13}C MRS to investigate tricarboxylic acid cycle flux in skeletal muscle. In comparison with ^{13}C, the T_1 relaxation times of the quadrupolar ^{2}H nuclei are about an order of magnitude shorter, allowing fast averaging in a 3D MRSI experiment. Moreover, there is no need for decoupling, which makes deuterium metabolic imaging extremely suited for application at ultrahigh field, with significant sensitivity gains.[13] However, thus far DMRSI has not yet been applied to skeletal muscle.

Skeletal muscle is a tissue with a high degree of spatial organization. In hydrogen-1 (^{1}H) MR spectra, this leads to residual dipolar coupling splittings for the resonances of Cr, taurine, and lactate as a result of incomplete motional averaging of the orientation-dependent (anisotropic) dipolar interactions.[14–22] For ^{2}H nuclei, next to the effects of dipolar couplings, we also have to consider the residual effects of the quadrupolar coupling when motion is not completely isotropic. Both from ab initio calculations and NMR experiments, the deuteron quadrupolar coupling constant (C_Q) for a deuterated water (HDO) molecule in a liquid environment has been determined to be ~250 kHz at body temperature.[23,24] In liquid water, this quadrupolar interaction is averaged. However, in macroscopically ordered tissues such as tendons, a residual quadrupolar interaction leads to a well-resolved splitting of the deuterated water signal[25]; whereas in locally ordered systems such as cartilage, line broadening has been observed.[26] In this study, we investigated the partial alignment of naturally abundant HDO in the lower leg muscles by studying the residual deuteron quadrupolar coupling and its dependence on the angle between the muscle fibers and the main magnetic field B_0, as determined by DTI.

2 | METHODS

2.1 | DMRSI: Hardware

DMRSI measurements of the lower leg muscles were performed at a 7 Tesla whole-body MRI system (Philips Healthcare, Best, The Netherlands) using a 8-channel body array consisting of four ^{2}H transmit/receive loop coils tuned at 45.7 MHz, combined with four ^{1}H transmit/receive fractionated dipole antennas[27] divided into a posterior and anterior element. The four ^{1}H dipole antennas were interfaced to four 2 kW peak-power amplifiers. The ^{2}H transmit/receive loops were interfaced to a 10 kW peak-power amplifier (AN8112, Analogic Corporation, Peabody, MA). The amplifier was driven at 4 kW output and then split into the 4 channels, resulting in 1 kW delivered peak power for the ^{2}H RF pulses to each coil.

2.2 | DMRSI: Data acquisition

The study was approved by the medical research ethics committee of the University Medical Center Utrecht (Utrecht, The Netherlands) (protocol number 15-466). After signing informed consent, 3 healthy male volunteers were scanned in a supine position, with the right leg parallel with the B_0 field and the 2 coil elements positioned below and above the right lower leg. One of the volunteers was scanned again in the same session, this time on the right side and with the right knee bent such that the angle between the right lower leg and B_0 was approximately 45° (as determined from the angle between the tibia bone and the *z*-axis on a coronal scan). Before the DMRSI experiments, after RF phase and B_0 shimming (see Supporting Information), transversal and coronal T_1-weighted (T_1w) images (multi-slice gradient echo, TE = 4.93 ms, TR = 10 ms, in-plane resolution = 0.5 × 0.5 mm^2, slice thickness = 10 mm, flip angle = 15°) and transversal Dixon images (2D multi-slice gradient echo, TE = 2.6 ms, ΔTE = 0.5 ms, TR = 10 ms, in-plane resolution = 1.3 × 1.3 mm^2, slice thickness = 10 mm, flip angle = 15°) were

acquired with the same FOV and the same number of slices as for the DMRSI measurements.

All of the DMRSI measurements were performed with a pulse-acquire sequence using a 0.5 ms block pulse, followed by phase-encoding gradients for 3D spatial encoding. A TR of 333 ms was used, and the signal was sampled with a 5000 Hz spectral bandwidth and 1024 spectral points. DMRSI acquisitions were made using a Hamming-weighted k-space acquisition pattern. DMRSI acquisition parameters for scans with the right leg parallel with the B_0 field: TE = 1.84 ms, voxel size = $14 \times 14 \times 25$ mm^3, matrix size = $10 \times 10 \times 12$, number of averages = 16, acquisition time = 20:37 min. For the scan with the lower leg at an angle of 45° with B_0, both T_1w images and DMRSI acquisition matrix were also angulated at 45° with respect to the B_0 field (anteroposterior). A larger FOV was chosen to avoid aliasing from the upper leg. DMRSI acquisition parameters for scan with lower leg at an angle of 45° with B_0: TE = 1.78 ms, voxel size = $15 \times 15 \times 25$ mm^3, matrix size = $10 \times 14 \times 12$, number of averages = 8, acquisition time = 17:26 min. During all scans, the foot was not flexed.

2.3 | DMRSI: Data reconstruction and analysis

Reconstruction and processing of the raw DMRSI data were performed with an in-house written MatLab (Version R2019a, MathWorks, Natick, MA) script. Channel combination was performed using the Roemer equal noise algorithm.[28] Spectra were denoised with a principal component analysis–noise suppression algorithm[29,30] and zero-filled to 2048 points. The linewidths and splittings of the HDO signal in each voxel were determined by fitting the signal with 2 Lorentzian lines, with equal linewidth, amplitude, and phase, using AMARES (Advanced Method for Accurate, Robust, and Efficient Spectral fitting).[31]

2.4 | DTI: Data acquisition and analysis

Because the deuterium body array is not optimal for ^{1}H MRI, DTI was performed on the same volunteers in the same positions using a Philips Ingenia 3 Tesla MRI scanner (Philips

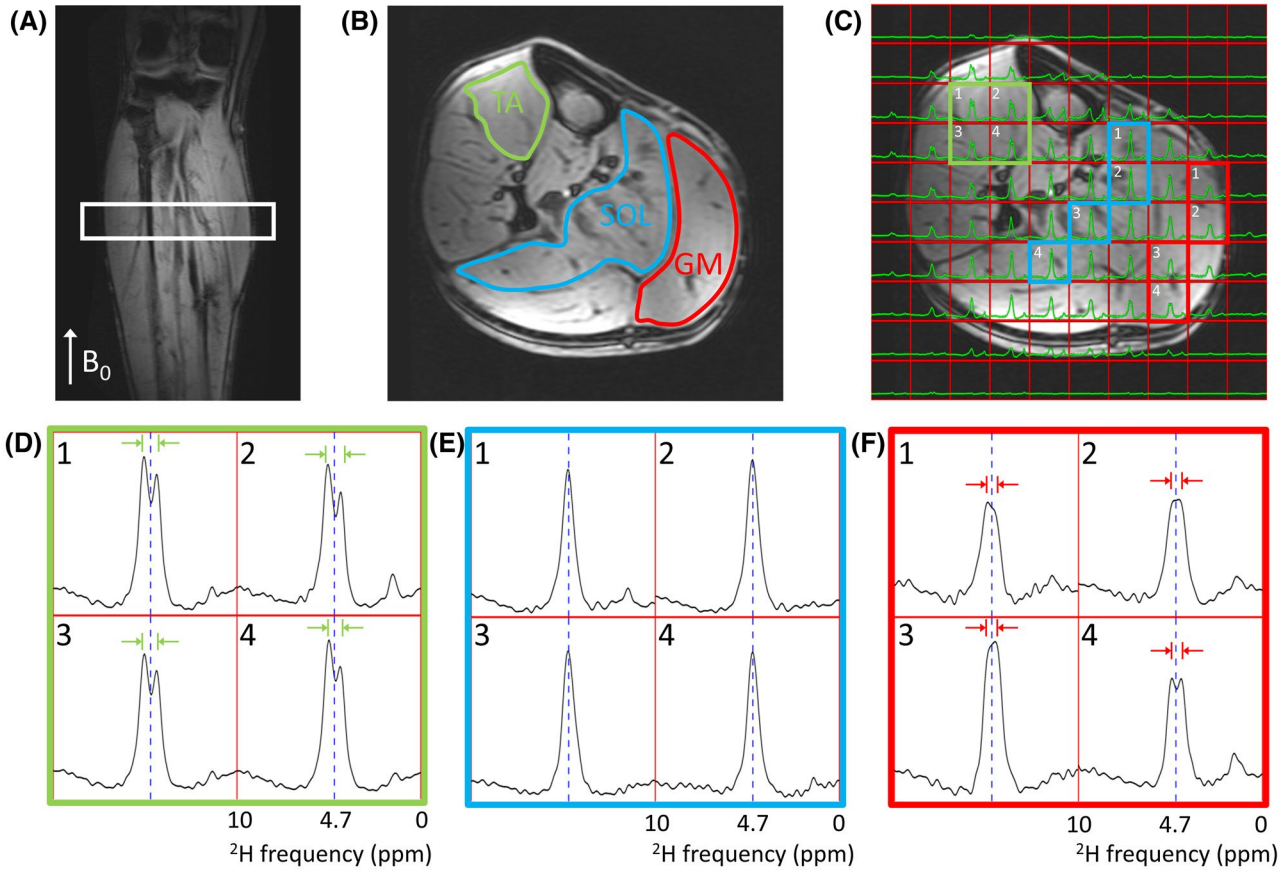

FIGURE 1 Natural abundance DMRSI data in the right lower leg (subject 1) positioned parallel with B_0. (A) Coronal T_1w image. The white rectangle indicates the slice shown in panels B and C. Transversal T_1w image with (B) segmentation of TA, SOL, and GM muscles, and (C) overlaid with DMRSI data. Spectra from selected voxels in TA (D), SOL (E), and GM (F), as indicated in panel C, showing the signal from HDO at 4.7 ppm (*x*-axis range: 0–10 ppm = 457 Hz). DMRSI, deuterium MRSI; GM, gastrocnemius medialis; HDO, deuterated water; SOL, soleus; TA, tibialis anterior; T_1w,T_1-weighted

Healthcare, Best, The Netherlands) and a 16-channel anterior and 12-channel posterior receive coil. DTI data was acquired using a single-shot spin-echo EPI sequence. The acquisition parameters were: TE = 57 ms; TR = 5000 ms; FOV = 480 × 276 × 150 mm^3; in-plane resolution = 3 × 3 mm^2; slice thickness = 6 mm; SENSE = 1.9; *b* values (number of directions) = 0 (1), 1 (6), 10 (3), 25 (3), 100 (3), 200 (6), 400 (8), and 600 (12) s/mm^2; fat suppression with SPectral Attenuated Inversion Recovery, Spectral Presaturation with Inversion Recovery, and gradient reversal. Data processing was performed using QMRITools (github.com/mfroeling/QMRITools).[32] The data was first denoised using a principal component analysis–noise suppression algorithm,[29] after which the data were corrected for motion and eddy currents. Next, intravoxel incoherent motion correction was performed,[33] and the tensor was calculated using an iterative weighted linear least-squares algorithm.[34] For each voxel, the angle of the principal eigenvector was calculated relative to the through plane vector. For each muscle, the average fiber angle was then calculated over a volume of interest, which corresponded to the voxels analyzed for the DMRSI data.

3 | RESULTS

Figure 1 shows the results of the DMRSI measurements from 1 of the subjects (subject 1), with the lower leg positioned parallel with B_0. The naturally abundant HDO signal could be detected in the 4.9 mL voxels with good sensitivity. Spectra from selected voxels in the tibialis anterior (TA), soleus (SOL), and gastrocnemius medialis (GM) muscles showed a distinctive pattern. The HDO signal in TA was clearly split. In GM, a splitting could also be observed, but it was smaller than in the TA. In SOL, no splitting could be resolved by eye. Splittings as determined from the AMARES fits (Supporting Information Figure S1) are reported in Table 1 for the 3 subjects. The size of the splittings was quite consistent among subjects for TA and GM, although a larger variation was observed in SOL. Mean splittings were 31.0 ± 0.5 Hz in TA, 20.9 ± 2.2 Hz in GM, and 15.1 ± 4.4 Hz in SOL. The splitting patterns for the different muscles did not change in the proximal-to-distal direction, as illustrated for the TA in Supporting Information Figure S2.

The results from the DMRSI measurement with the lower leg at an angle of approximately 45° with B_0 (subject 1) are shown in Figure 2. In this orientation, no splittings could be observed in any of the 3 muscles. Calculated splittings from the AMARES fits were 8.8 ± 1.6 Hz for TA, 10 ± 1.1 Hz for SOL, and 10.3 ± 1.5 for GM, respectively, which are much smaller than the fitted linewidths (Table 1). For the TA and GM muscles, the difference in spectral appearance between the 2 orientations can be appreciated from an overlay of the spectra from the 2 scans of subject

TABLE 1 Splittings and linewidths of the HDO signal in the DMRSI spectra determined from AMARES fits, and muscle fiber angles determined from DTI measurements

		Parallel with B_0			45° with Respect to B_0		
	Muscle	Splitting (Hz)	Linewidth (Hz)	Fiber Angle	Splitting (Hz)	Linewidth (Hz)	Fiber Angle
Subject 1	TA	31.4 ± 1.0	27.9 ± 0.3	24.7° ± 10.7°	8.8 ± 1.6	26.2 ± 2.8	62.9° ± 8.6°
	SOL	12.6 ± 1.8	29.0 ± 3.1	43.4° ± 15.6°	10.0 ± 1.1	27.7 ± 1.9	74.2° ± 10.2°
	GM	23.4 ± 1.8	29.5 ± 1.6	32.4° ± 6.6°	10.3 ± 1.5	29.8 ± 4.9	45.0° ± 17.7°
Subject 2	TA	31.2 ± 0.9	29.0 ± 0.5	27.8° ± 12.8°	–	–	–
	SOL	12.5 ± 2.0	30.5 ± 1.1	33.9° ± 8.6°	–	–	–
	GM	19.0 ± 2.3	32.3 ± 0.9	26.7° ± 8.7°	–	–	–
Subject 3	TA	30.4 ± 2.0	36.1 ± 2.1	13.6° ± 7.8°	–	–	–
	SOL	20.3 ± 0.8	33.3 ± 2.6	20.4° ± 8.9°	–	–	–
	GM	20.5 ± 0.8	33.8 ± 2.5	19.4° ± 4.5°	–	–	–
Mean	TA	31.0 ± 0.5	31.0 ± 1.0	22.0° ± 7.5°	–	–	–
	SOL	15.1 ± 4.4	30.9 ± 2.3	32.6° ± 11.5°	–	–	–
	GM	20.9 ± 2.2	31.8 ± 1.7	26.2° ± 6.5°	–	–	–

Data are means ± SD. Values are reported for the TA, SOL, and GM muscles when the lower leg was parallel with B_0 (3 subjects) and at an angle of approximately 45° with respect to B_0 (1 subject). For each muscle and each orientation, n = 11–12 voxels were analyzed from 3 transversal slices of each DMRSI data set (n = 4 voxels from each slice, except for 1 of the slices from subject 3, for which only n = 3 voxels did fit in the GM muscle). The volumes of interest used to determine the mean muscle fiber angles from the DTI data corresponded with the voxels analyzed for the DMRSI data.

Abbreviations: AMARES, Advanced Method for Accurate, Robust, and Efficient Spectral fitting; DMRSI, deuterium MRSI; HDO, deuterated water; GM, gastrocnemius medialis; SOL, soleus; TA, tibialis anterior.

1 for a selected voxel, whereas the spectra from a voxel in the SOL are very similar for the 2 orientations (Supporting Information Figure S3).

Figure 3 shows the DTI results of subject 1 for both positions of the lower leg. Muscle fiber tracking results are shown for TA, SOL, and GM (Figure 3A,B). Average muscle fiber angles calculated within volumes of interest corresponding to the DMRSI voxels are reported in Table 1, and the mean values for the 3 subjects were 22.0° ± 7.5° for TA, 32.6° ± 11.5° for SOL, and 26.2° ± 6.5° for GM, respectively, when the lower leg was parallel to B_0. When the lower leg (subject 1) was at an angle of approximately 45° with B_0, average fiber angles became 62.9° ± 8.6° for TA, 74.2° ± 10.2° for SOL, and 45.0° ± 17.7° for GM, respectively (Figure 3D,F).

Figure 4 shows color maps of the muscle fiber angles in subject 1, with the leg positioned parallel with B_0, together with maps of the residual quadrupolar splittings (in Hz) fitted from the DMRSI data. In addition, maps were created based on the theoretical relationship (see Discussion section) between muscle fiber angles and residual quadrupolar splittings according to the formula $\Delta\nu = |C\left(3cos^2\theta - 1\right)|$, where θ is the muscle fiber angle and C is a constant.

4 | DISCUSSION

In this study, we measured deuterium MR spectra of the lower leg muscles at 7 Tesla, and we observed splittings in the natural abundance HDO signal in some but not all muscles. Furthermore, the size of the splittings varied between different muscles in the lower leg and depended on the orientation of the leg in the MRI scanner.

Deuterium is a quadrupolar nucleus and has an associated quadrupolar coupling with the local electric field gradient. Both from ab initio calculations and NMR experiments, the deuteron quadrupolar coupling constant of deuterated water in a liquid environment has been determined to be ~250 kHz at body temperature.[23,24] In

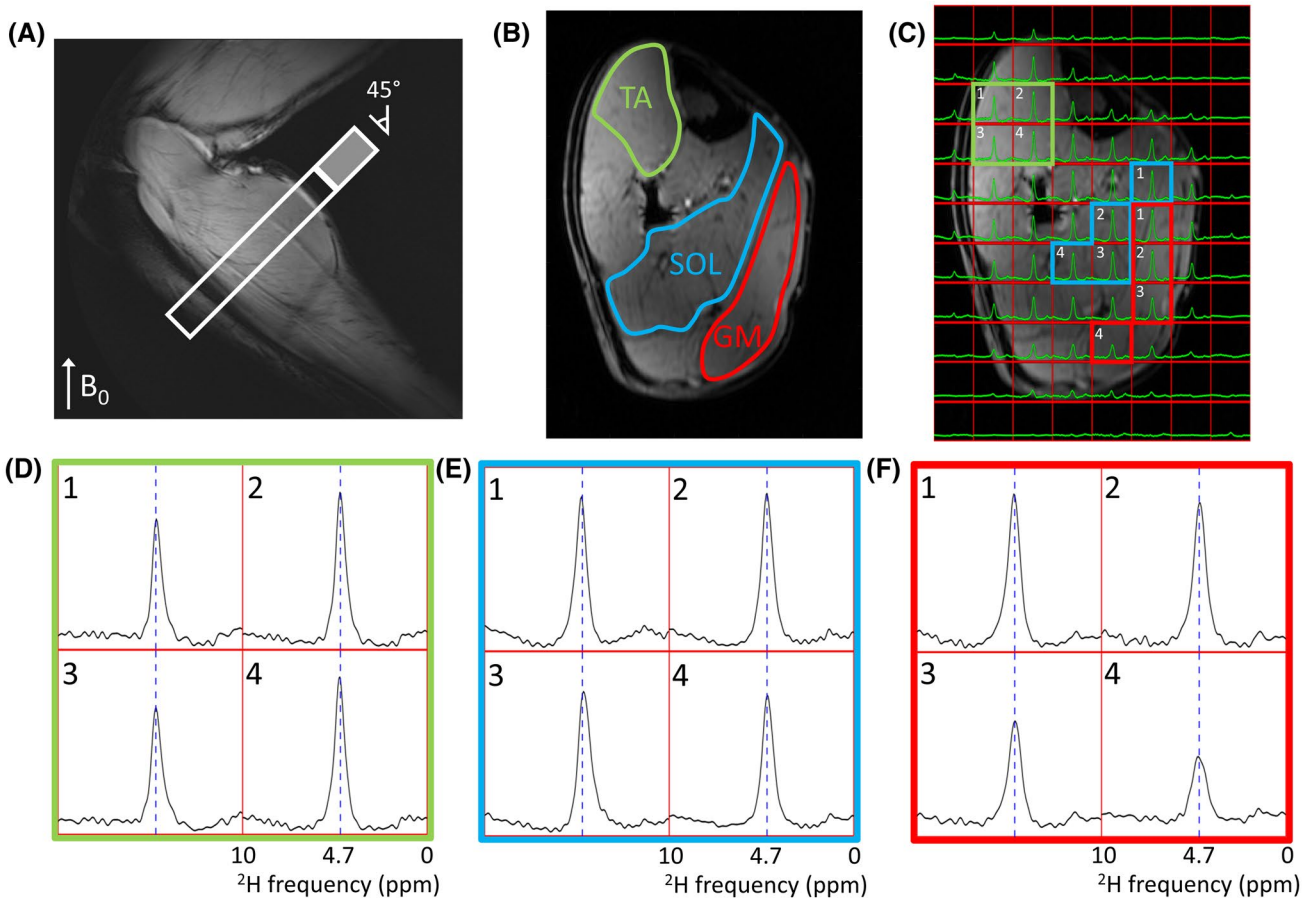

FIGURE 2 Natural abundance DMRSI data in the right lower leg (subject 1) positioned at an angle of approximately 45° with respect to B_0. (A) Sagittal T_1w image. The white rectangle indicates the slice shown in panels B and C (cropped in the AP direction to the size of open part of rectangle). Transversal T_1w image with (B) segmentation of TA, SOL, and GM muscles, and (C) overlaid with DMRSI data. Spectra from selected voxels in TA (D), SOL (E), and GM (F), as indicated in panel C, showing the signal from HDO at 4.7 ppm (*x*-axis range: 0–10 ppm = 457 Hz). AP, anteroposterior

in vivo deuterium MR spectra of brain, liver, tumor, and brown adipose tissue,[1–4] quadrupolar splittings have not been observed because the quadrupolar interactions are averaged due to fast, isotropic rotational tumbling. However, in an ex vivo sample of macroscopically ordered bovine Achilles tendon, immersed in D_2O, a well-resolved splitting of the deuterated water signal could be detected by deuterium double-quantum–filtered NMR spectroscopy.[25] Recently, similar experiments were performed on ex vivo spinal cord in which 5 different water compartments were identified from the deuterium double-quantum–filtered spectra.[35] The most prominent deuterated water signal showed a residual quadrupolar splitting of about 550 Hz and was assigned to the myelin water. This splitting was invariant with respect to the orientation of the spinal cord relative to the magnetic field, indicating that myelin acts as a liquid crystalline medium, which orients itself with respect to the magnetic field and not with the spinal cord. The splitting of the signal from another, smaller compartment (~1500 Hz) was found to be orientation-dependent and was assigned to collagenous connective tissue.

Skeletal muscle also has a high degree of spatial organization, resulting in incomplete motional averaging. This effect is well known from ^{1}H MR spectra of skeletal muscle, in which residual dipolar couplings can be observed for the resonances of Cr, taurine, and lactate[14–16,20–22] due to not completely isotropic motion of the molecules. The splittings due to these residual dipolar couplings appeared to be orientation-dependent, and it was shown that the residual dipolar couplings are proportional to the angle θ between the muscle fibers and the main magnetic field B_0 according to $3\cos^2\theta - 1$.[14–17,19–22]

We observed the same orientation dependence for the splittings of the HDO deuterium signal in skeletal muscle (Figure 1). These splittings will originate mainly from the residual deuteron quadrupolar coupling, which is typically an order of magnitude larger than the dipolar couplings. Moreover, residual dipolar couplings tend to average out due to chemical exchange between protons/deuterons between water molecules.[35] The sizes of the observed splittings (the largest splitting was observed in TA when the lower leg was positioned parallel with B_0, with a mean of 31.0 ± 0.5 Hz among the 3 subjects) are only a fraction of the deuteron quadrupolar coupling constant of ~250 kHz in liquid water[23,24] and are also smaller than the splittings observed in tendon and spinal cord.[25,35] This indicates only a very small preferential alignment of the HDO molecules in the muscle fibers, which can be described by an alignment tensor that describes the average

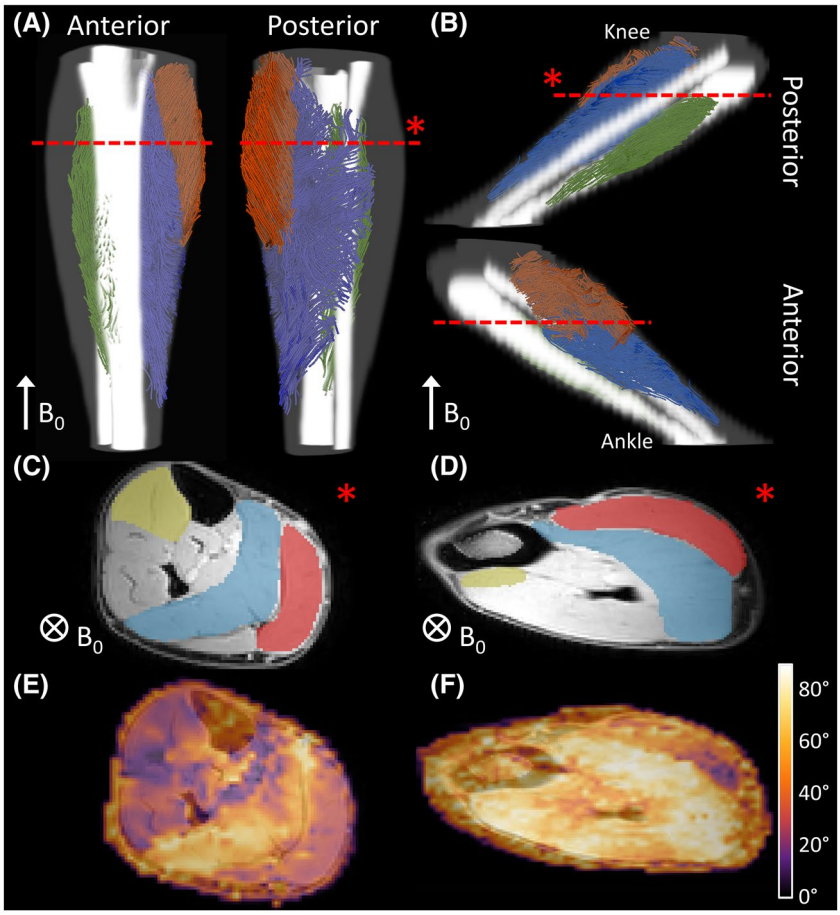

FIGURE 3 Muscle fiber tracking results from DTI data in the right lower leg (subject 1), positioned parallel with B_0 (A,C,E) and at an angle of approximately 45° with respect to B_0 (B,D,F). (A,B) Illustration of muscle fibers of TA (green), SOL (blue), and GM (red) for 2 different viewpoints. (C,D) Transversal Dixon water images at the positions indicated by the red dashed lines in panels (A,B), with segmentation masks for the whole TA, SOL, and GM muscles. Of note, these are not the volumes of interest for which mean muscle fiber angles are reported in Table 1. (E,F) Color maps of calculated muscle fiber angles (in degrees) with respect to the through plane vector overlaid on Dixon water images

orientation of the molecule with respect to the magnetic field. The observed quadrupolar splitting will depend on the alignment and the quadrupolar interaction parameters C_Q and η_Q. The principal axis of the deuterium electric field gradient tensor lies along the O–D internuclear vector. If we neglect the small asymmetry parameter η_Q~0.12, the quadrupolar splitting can be written as $\Delta\nu_Q = \frac{3}{4}C_Q(3\cos^2\theta_{OD} - 1)$, which is a quantity depending on the geometrical term and the motional averaging. The principal axis of the electric field gradient tensor is expected to be very slightly aligned with the muscle fibers. Thus, similar to the residual dipolar couplings observed in ^{1}H MR spectra of skeletal muscle, the residual deuteron quadrupolar coupling in HDO in muscle is expected to depend on the angle θ between the muscle fibers and the main magnetic field B_0 and is proportional to $3\cos^2\theta - 1$, which becomes 0 at the magic angle of 54.7°.

To determine muscle fiber angles, we acquired DTI data from the same volunteers in the same positions. When the lower leg was parallel with B_0, the muscle fibers in TA run almost parallel with B_0 (Figure 3) (Table 1). The TA also showed the largest residual quadrupolar splittings in the deuterium spectra for all subjects (Figure 1) (Table 1), irrespective of the proximodistal position (Supporting Information Figure S2). In contrast, when the lower leg was parallel with B_0, the muscle fibers in SOL are closest to the magic angle. In accordance, no resolved splitting could be observed in the deuterium spectra from SOL for subjects 1 and 2. However, muscle fiber angles in SOL were more variable among the subjects, which has also been observed in previous DTI studies.[36] In subject 3, with the smallest fiber angles in SOL, a splitting was visible in the deuterium spectra from SOL. For subjects 1 and 2, the splittings in GM were smaller than in TA and larger than in SOL; whereas in subject 3, splittings were similar in GM and SOL. In Figure 4, color maps of the fitted residual quadrupolar splittings in several transversal slices for subject 1 are compared with coregistered maps of muscle fiber angles and the derived $\Delta\nu = |C\left(3cos^2\theta - 1\right)|$ maps, from which the spatial correlation can be clearly appreciated.

When the lower leg was positioned at an angle of approximately 45° with B_0, no resolved splittings could be observed in any of the 3 muscles (Figure 2), and fitted splittings were much smaller than the linewidths (Table 1). For the muscle fibers in TA, which run more or less parallel with respect to the tibia bone, the average angle between the muscle fibers and B_0 (62.9° ± 8.6°) approached the magic angle in this orientation. Also for GM, the average angle was close to the magic angle in this orientation, whereas for SOL the average angle between the muscle fibers and B_0 (74.2° ± 10.2°) became larger than the magic angle. However, due to the $3\cos^2\theta - 1$ relationship, the residual quadrupolar couplings are expected to be smaller at angles larger than the magic angle than at angles smaller than the magic angle. Although for the DMRSI scan with the leg positioned at an angle of 45° the voxel size in the transversal plane was slightly increased from 14×14 mm^2 to 15×15 mm^2, averaging over slightly more muscle fibers will probably have had a negligible effect on the results.

Therefore, the sizes of the observed deuterium quadrupole splittings in the different muscles and in the different orientations are in good agreement with the expected

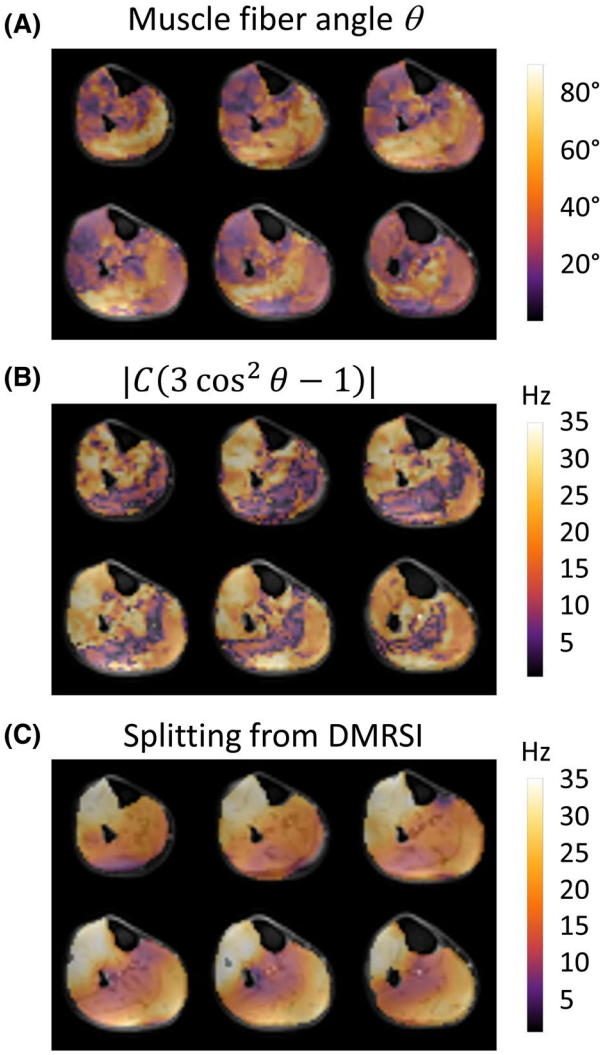

FIGURE 4 Color maps of (A) calculated muscle fiber angles (in degrees) with respect to the through plane vector, (B) residual quadrupolar splittings (in Hz) calculated from the muscle fiber angles θ using the formula $\Delta\nu = |C\left(3\cos^2\theta - 1\right)|$ with C = 16.5 Hz , and (C) residual quadrupolar splittings (in Hz) fitted from the DMRSI data, for 6 consecutive transversal slices overlaid on Dixon water images. The 7T DMRSI data and 3T DTI data were obtained in the right lower leg (subject 1) positioned parallel with B_0 and were coregistered based on Dixon images. The maps of residual quadrupolar splittings fitted from the DMRSI data (C) were extrapolated to the same resolution as the muscle fiber angle maps. T, Tesla

orientation dependence of the residual deuteron quadrupolar coupling in HDO. Deuterium is not the only quadrupolar nucleus for which splittings are observed in human muscle tissue. Rösler et al. made a similar observation in ^{39}K MR spectra of the thigh and calf.[37] ^{39}K is a spin 3/2 nucleus, and its interaction with nonvanishing local electric field gradients theoretically leads to 3 peaks, namely an unshifted central line and 2 satellites equally shifted to both sides. Rösler et al. showed that, although in brain tissue and in an agar phantom only a single ^{39}K peak was observed, in thigh and calf muscles 2 satellite peaks were visible, which were shifted by about +200 and −200 Hz. Although the measurements were unlocalized, and therefore different muscles with different muscle fiber orientations contributed to the signal, the ^{39}K splittings in the calf had an angular dependence with respect to the magnetic field B_0 similar to what we observed for deuterium. Using double-quantum filtering with magic-angle excitation, they could unequivocally show that the ^{39}K satellite signals in muscle tissue are caused by an anisotropic environment.

5 | CONCLUSION

In conclusion, partial molecular alignment in skeletal muscle leads to residual deuteron quadrupolar couplings in HDO, the size of which depends on the angle between the muscle fibers and B_0. This effect is also expected for signals from deuterated glucose, acetate, glutamate, and lactate, leading to further broadening of the inherently broad deuterium signals, which could reduce the spectral resolution of muscle deuterium spectra.

ORCID

Martijn Froeling https://orcid.org/0000-0003-3841-0497
Arjan D. Hendriks https://orcid.org/0000-0002-0363-2471
Jeanine J. Prompers https://orcid.org/0000-0002-4756-4474

REFERENCES

1. De Feyter HM, Behar KL, Corbin ZA, et al. Deuterium metabolic imaging (DMI) for MRI-based 3D mapping of metabolism in vivo. *Sci Adv*. 2018;4:eaat7314.
2. Lu M, Zhu XH, Zhang Y, Mateescu G, Chen W. Quantitative assessment of brain glucose metabolic rates using in vivo deuterium magnetic resonance spectroscopy. *J Cereb Blood Flow Metab*. 2017;37:3518-3530.
3. Kreis F, Wright AJ, Hesse F, Fala M, Hu DE, Brindle KM. Measuring tumor glycolytic flux in vivo by using fast deuterium MRI. *Radiology*. 2020;294:289-296.
4. Riis-Vestergaard MJ, Laustsen C, Mariager CØ, Schulte RF, Pedersen SB, Richelsen B. Glucose metabolism in brown adipose tissue determined by deuterium metabolic imaging in rats. *Int J Obes*. 2020;44:1417-1427.
5. De Feyter HM, Thomas MA, Behar KL, de Graaf RA. NMR visibility of deuterium-labeled liver glycogen in vivo. *Magn Reson Med*. 2021;86:62-68.
6. Hesse F, Somai V, Kreis F, Bulat F, Wright AJ, Brindle KM. Monitoring tumor cell death in murine tumor models using deuterium magnetic resonance spectroscopy and spectroscopic imaging. *Proc Natl Acad Sci USA*. 2021;118:e2014631118.
7. von Morze C, Engelbach JA, Blazey T, et al. Comparison of hyperpolarized 13C and non-hyperpolarized deuterium MRI approaches for imaging cerebral glucose metabolism at 4.7 T. *Magn Reson Med*. 2021;85:1795-1804.
8. Lebon V, Dufour S, Petersen KF, et al. Effect of triiodothyronine on mitochondrial energy coupling in human skeletal muscle. *J Clin Invest*. 2001;108:733-737.
9. Petersen KF, Befroy D, Dufour S, et al. Mitochondrial dysfunction in the elderly: possible role in insulin resistance. *Science*. 2003;300:1140-1142.
10. Petersen KF, Dufour S, Befroy D, Garcia R, Shulman GI. Impaired mitochondrial activity in the insulin-resistant offspring of patients with type 2 diabetes. *N Engl J Med*. 2004;350:664-671.
11. Befroy DE, Petersen KF, Dufour S, et al. Impaired mitochondrial substrate oxidation in muscle of insulin-resistant offspring of type 2 diabetic patients. *Diabetes*. 2007;56:1376-1381.
12. Befroy DE, Petersen KF, Dufour S, Mason GF, Rothman DL, Shulman GI. Increased substrate oxidation and mitochondrial uncoupling in skeletal muscle of endurance-trained individuals. *Proc Natl Acad Sci USA*. 2008;105:16701-16706.
13. Graaf RA, Hendriks AD, Klomp DWJ, et al. On the magnetic field dependence of deuterium metabolic imaging. *NMR Biomed*. 2020;33:e4235.
14. Vermathen P, Boesch C, Kreis R. Mapping fiber orientation in human muscle by proton MR spectroscopic imaging. *Magn Reson Med*. 2003;49:424-432.
15. Boesch C, Kreis R. Dipolar coupling and ordering effects observed in magnetic resonance spectra of skeletal muscle. *NMR Biomed*. 2001;14:140-148.
16. Kreis R, Boesch C. Liquid-crystal-like structures of human muscle demonstrated by in vivo observation of direct dipolar coupling in localized proton magnetic resonance spectroscopy. *J Magn Reson Ser B*. 1994;104:189-192.
17. Kreis R, Koster M, Kamber M, Hoppeler H, Boesch C. Peak assignment in localized 1H MR spectra of human muscle based on oral creatine supplementation. *Magn Reson Med*. 1997;37:159-163.
18. Kreis R, Boesch C. Spatially localized, one- and two-dimensional NMR spectroscopy and in vivo application to human muscle. *J Magn Reson B*. 1996;113:103-118.
19. Hanstock CC, Thompson RB, Trump ME, Gheorghiu D, Hochachka PW, Allen PS. Residual dipolar coupling of the CR/PCr methyl resonance in resting human medial gastrocnemius muscle. *Magn Reson Med*. 1999;42:421-424.
20. Ntziachristos V, Kreis R, Boesch C, Quistorff B. Dipolar resonance frequency shifts in 1H MR spectra of skeletal muscle: confirmation in rats at 4.7 T in vivo and observation of changes postmortem. *Magn Reson Med*. 1997;38:33-39.

21. in 't Zandt HJ, Klomp DW, Oerlemans F, Wieringa B, Hilbers CW, Heerschap A. Proton MR spectroscopy of wild-type and creatine kinase deficient mouse skeletal muscle: dipole-dipole coupling effects and post-mortem changes. *Magn Reson Med*. 2000;43:517-524.
22. Asllani I, Shankland E, Pratum T, Kushmerick M. Anisotropic orientation of lactate in skeletal muscle observed by dipolar coupling in 1H NMR spectroscopy. *J Magn Reson*. 1999;139:213-224.
23. Struis RPWJ, De Bleijser J, Leyte JC. Dynamic behavior and some of the molecular properties of water molecules in pure water and in MgCl2 solutions. *J Phys Chem*. 1987;91:1639-1645.
24. Ludwig R, Weinhold F, Farrar TC. Experimental and theoretical determination of the temperature dependence of deuteron and oxygen quadrupole coupling constants of liquid water. *J Chem Phys*. 1995;103:6941-6950.
25. Eliav U, Navon G. A study of dipolar interactions and dynamic processes of water molecules in tendon by 1H and 2H homonuclear and heteronuclear multiple-quantum-filtered NMR spectroscopy. *J Magn Reson*. 1999;137:295-310.
26. Sharf Y, Eliav U, Shinar H, Navon G. Detection of anisotropy in cartilage using 2H double-quantum-filtered NMR-spectroscopy. *J Magn Reson B*. 1995;107:60-67.
27. Raaijmakers AJE, Italiaander M, Voogt IJ, et al. The fractionated dipole antenna: a new antenna for body imaging at 7 Tesla. *Magn Reson Med*. 2016;75:1366-1374.
28. Roemer PB, Edelstein WA, Hayes CE, Souza SP, Mueller OM. The NMR phased array. *Magn Reson Med*. 1990;16:192-225.
29. Veraart J, Novikov DS, Christiaens D, Ades-Aron B, Sijbers J, Fieremans E. Denoising of diffusion MRI using random matrix theory. *Neuroimage*. 2016;142:394-406.
30. Froeling M, Prompers JJ, Klomp DWJ, van der Velden TA. PCA denoising and Wiener deconvolution of 31P 3D CSI data to enhance effective SNR and improve point spread function. *Magn Reson Med*. 2021;85:2992-3009.
31. Vanhamme L, Van Den Boogaart A, Van Huffel S. Improved method for accurate and efficient quantification of MRS data with use of prior knowledge. *J Magn Reson*. 1997;129:35-43.
32. Froeling M. QMRTools: a Mathematica toolbox for quantitative MRI analysis. *J Open Source Softw*. 2019;4:1204.
33. De Luca A, Bertoldo A, Froeling M. Effects of perfusion on DTI and DKI estimates in the skeletal muscle. *Magn Reson Med*. 2017;78:233-246.
34. Veraart J, Sijbers J, Sunaert S, Leemans A, Jeurissen B. Weighted linear least squares estimation of diffusion MRI parameters: strengths, limitations, and pitfalls. *Neuroimage*. 2013;81:335-346.
35. Eliav U, Shinar H, Navon G. Identification of water compartments in spinal cords by 2H double quantum filtered NMR. *NMR Biomed*. 2021;34:e4452.
36. Schlaffke L, Rehmann R, Rohm M, et al. Multi-center evaluation of stability and reproducibility of quantitative MRI measures in healthy calf muscles. *NMR Biomed*. 2019;32:e4119.
37. Rösler MB, Nagel AM, Umathum R, Bachert P, Benkhedah N. In vivo observation of quadrupolar splitting in 39K magnetic resonance spectroscopy of human muscle tissue. *NMR Biomed*. 2016;29:451-457.

SUPPORTING INFORMATION

Additional Supporting Information may be found in the online version of the article at the publisher's website.

FIGURE S1 AMARES fit results for selected voxels in the Tibialis Anterior (TA; green box), Soleus (SOL; blue box) and Gastrocnemius Medialis (GM; red box) muscles, for the deuterium MRSI (DMRSI) data set with the lower leg positioned parallel with B_0. The upper row shows the original spectrum in black, the fitted signal in blue and the residual in red. The rows below show the fitted components, i.e. two Lorentzian lines for deuterated water (HDO-1 and HDO-2), with equal linewidth, amplitude and phase, and one Lorentzian line for the signal from deuterated lipids

FIGURE S2 (A) Coronal T_1w image of the right lower leg (subject 1) overlaid with the DMRSI acquisition grid and (B) DMRSI data from the same coronal slice, showing the signal from HDO in muscle at 4.7 ppm and the signal from deuterated lipids in bone marrow and subcutaneous fat at 1.3 ppm (x-axis range: 0–10 ppm = 457 Hz). The TA muscle is delineated with a green line in both panels

FIGURE S3 Overlay of spectra from the scans with the lower leg (subject 1) positioned parallel with B_0 (in black) and with the lower leg positioned at an angle of approximately 45° with respect to B_0 (in red), for selected voxels in the TA (green box), SOL (blue box) and GM (red box)

How to cite this article: Gursan A, Froeling M, Hendriks AD, et al. Residual quadrupolar couplings observed in 7 Tesla deuterium MR spectra of skeletal muscle. *Magn Reson Med*. 2022;87:1165–1173. doi:10.1002/mrm.29053